UTILIZATION OF METAKAOLIN AND BLAST FURNACE SLAG IN AUTOCLAVED AERATED CONCRETE PRODUCTION

KADIR GÜÇLÜER[1]*, İSMAIL DEMIR[2]
[1]*Afyon Kocatepe University, Graduate School of Natural and Applied Science, Civil Engineering Dept., Afyonkarahisar, Turkey.*
[2]*Afyon Kocatepe University, Engineering Faculty, Department of Civil Engineering, Afyonkarahisar, Turkey.*

This study aimed to use metakaolin and blast furnace slag as main raw materials in the production of autoclaved aerated concrete (AAC). AAC is a light building material obtained by bringing of silica sand, cement, gypsum, lime and pore-forming agent together and hardening it in autoclave. In this study, instead of silica sand, samples of AAC were produced using metakaolin and blast furnace slag (BFS). Experimental measurements were carried out to determine the physical, mechanical and thermal properties of the AAC samples. The micro structural investigations were carried out using SEM and XRD technique.

Keywords: *Autoclaved aerated concrete, Metakaolin, Blast Furnace Slag, Microstructure, Mechanical Properties*

1. Introduction

Autoclaved aerated concrete (AAC) has been widely used in construction of load-bearing and non-load-bearing walls [1]. Compared with conventional construction materials, AAC offers lower density, lower thermal conductivity, lower shrinkage, greater fire resistance and ease of use in construction [2]. In general, the raw materials are cement, lime, gypsum, quartz sand and metallic Al powder (forming hydrogen gas) and the porosity of AAC which is around of 80% [3]. These components are mixed with high amounts of water and molded to produce a cellular green body by H_2 gas generation at atmospheric pressure, and then autoclaved at 200^{0}C under saturated steam pressure for several hours [4]. The aluminum powder reacts with calcium hydroxide to form hydrogen gas in the making of aerated concrete, as follows (Equation 1) [5].

$$2Al+3Ca(OH)_2+6H_2O \rightarrow 3CaO\ Al_2O_3\ 6H_2O + 3H_2 \quad (1)$$

The specific surface area of the quartz sand plays an important role in the production of autoclaved concrete, in most cases the quartz sand is ground to the required fineness by ball mill. This process is energy consuming. Many studies have been reported that the hydrothermal reactions in the $CaO\text{-}SiO_2\text{-}H_2O$ system are controlled by the dissolution of quartz; the results showed that finer sand reduces AAC processing time [6]. There is a growing interest in the use of mineral admixtures for cement [7]. Supplementary cementations materials have been increasingly used in the preparation of AAC [8]. Metakaolin (MK) has been successfully used as a supplementary cementitous material (SCM) in concrete since 1990 [9]. MK is produced by calcination of kaolin at 650–800 ^{0}C. The main components of MK are amorphous Al_2O_3 and SiO_2 [10]. The particle size of metakaolin is smaller than cement particles [11].

Slags is a by-product of pyro-metallurgical process in the metal and alloy industries [12]. The blast furnace generally works at 1500 ^{0}C. The slag in the molten form from the blast furnace is rapidly cooled with powerful water jets, which turned the molten slag into a fine, granular and glassy form known as granulated blast furnace slag [13].

Several researchers have investigated the potentiality of replacing of the traditional raw materials in AAC production by industrial wastes, such as fly ash [14], rice husk ash [15], waste glass [16], silica fume [17] and copper tailings [18]. In the literature, there is not much data on the use of metakaolin and BFS in AAC production. In this study, metakaolin and BFS used as mainly raw materials to produce AAC. The aim of this work is to investigate the physical, mechanical, thermal and microstructural properties of the AAC produced from metakaolin and BFS.

2. Materials and Methods

2.1 Materials

The AAC samples were prepared by the following materials; MK, BFS, gypsum, lime, water, foaming agent (Al powder). Metakaolin by a firm in

* Autor corespondent/*Corresponding author*,
E-mail: kgucluer@adiyaman.edu.tr

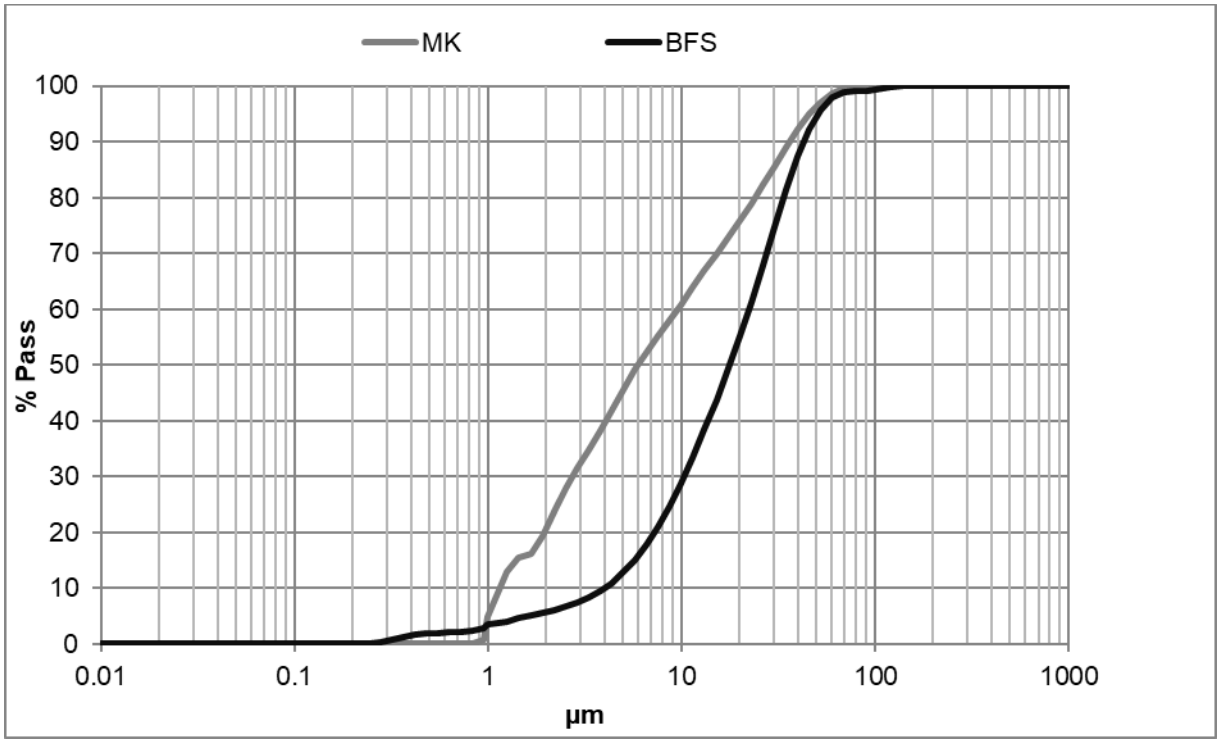

Fig. 1 - Laser particle size distribution of the MK and BFS.

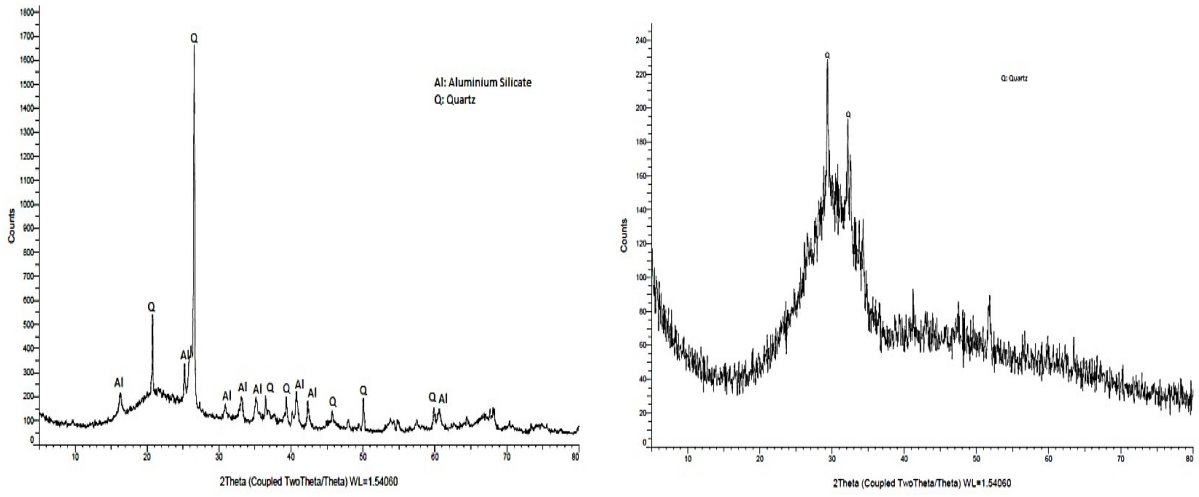

(a) (b)

Fig. 2 - XRD analysis of the MK (a) and BFS (b).

Turkey was imported from India. BFS was obtained from OYAK corporation in Turkey. Cement was appropriate to the TS EN 197-1 [19] CEM I 42.5 R. The chemical composition and Blaine fineness of cement, metakaolin and BFS are given in Table 1. Blaine fineness values of the samples were measured in Niğde Ömer Halis Demir University Construction Materials Laboratory in Turkey. MK, BFS and cement Blaine fineness (BF) were 12882 cm^2/gr, 2695 cm^2/gr and 3074 cm^2/gr respectively. Laser particle size distribution of the MK and BFS are given in Figure 1.

The diameter distribution of metakaolin was determined as d_{10} = 1.188 µm, d_{50} = 5.957 µm and

Table 1

Chemical composition and Blaine fineness of the materials

Oxides (Wt %)	MK	BFS	Cement
SiO_2	54	40.1	19.2
Al_2O_3	42	12.8	3.88
Fe_2O_3	0.35	0.9	4.25
CaO	0.01	39.6	62.8
MgO	0.06	4.2	3.42
K_2O	0.2	1.2	0.34
Na_2O	0.13	0.05	2.1
Blaine Fineness (cm^2/gr)	12882	2695	3074

d_{90} = 36.175 μm and the diameter distribution of BFS was determined as d_{10} = 3.985 μm, d_{50} = 17.635 μm and d_{90} = 42.623 μm. Mineralogical analysis of the MK and BFS appreciated by RX diffraction analyse (Figure 2).

As a result of mineralogical examination of metakaolin, aluminum silicate and quartz peaks were found in crystal structure. By XRD analysis of the BFS it has been found to be amorphous. In particular, the hump region in the $2\Theta = 20^0$ and 30^0 is amorphous. In addition, quartz peaks were observed in the BFS.

2.2 Methods

For mixtures production, mineral materials, cement and gypsum, which are primarily used, were subjected to dry mixing. After the mixture becomes homogeneous, it is added to the water and the ingredients are mixed with the aid of the mixer. After the consistency of the mixture is ready, the mixture of quicklime and aluminum dust is added and mixed with a mixer for 1-2 minutes. The mixture was then placed in preformed cube molds of 7 cm diameter to fill 2/3 of the mold height. The samples placed in the molds were left in the oven set at 75 ^{0}C for 1 hour to continue their swelling and hardening. The samples were then removed from the molds and cured for 8 hours under an 8 bar vapor pressure in an autoclave at 172 ° C, ready for physical and mechanical experiments (Figure 3).

The bulk density of the samples was measured by simply dividing the mass of the samples to their volumes. Bulk density have been determined by oven dry at 105 ± 5 ^{0}C until tested samples have been reached a constant mass. Compressive strength has been performed on AAC samples at loading rate of 2.0 ± 0.5 kgf/cm^2/s and on AAC samples. The mineralogical characteristics of the samples were investigated by XRD technique. SEM technique was used to identify the microstructural characteristics. The thermal conductivity coefficient measurements on selected samples were made according to ASTM C 1113-90 [20]. The apparent porosity values of the samples was determined according to TS EN 772-4 standard [21]. Mixing ratios of AAC samples are given in Table 2.

Fig. 3 - Experiment samples.

3. Results and Discussion

The bulk density and compressive strength data of mixtures composed of different components are given in Figure 4.

It has been found that in all series, when the cement ratio decreases in the mixture, the compressive strength decreases. High-cement ratio, bringing more create cement paste that means strength growth together. The compressive strength values of the samples produced with BFS are higher than the compressive strength values of the samples produced with MK. BFS 1 series of compressive strength 3.28 MPa, the bulk density 630 kg/m^3 while MK1 series of compressive strength 1.55 MPa, the bulk density 490 kg/m^3 were determined. Huang et al., [17], they found that the compressive strength of AAC samples was 4,0 MPa with a bulk density of 610 kg/m^3, which they produced using BFS as cement substitute. These data are similar to the results found in the literature. Compressive strength is closely related to its bulk density [22] which is mainly controlled by the dosage of aerating agent and the specific gravity of constituent materials [23].

Table 2

Mixing ratios of aerated concrete samples (by weight units)

Series	C	M	S	G	L	W	Al
MK1	0.8	1.5	-	0.3	0.3	3.0	0.001
MK2	0.7	1.5	-	0.3	0.3	3.0	0.001
MK3	0.6	1.5	-	0.3	0.3	3.0	0.001
BFS1	0.8	-	1.5	0.3	0.3	2.0	0.001
BFS2	0.7	-	1.5	0.3	0.3	2.0	0.001
BFS3	0.6	-	1.5	0.3	0.3	2.0	0.001

(C: cement, M: metakaolin, S: blast furnace slag, G: gypsum, L: lime, W: water, Al: aluminum powder).

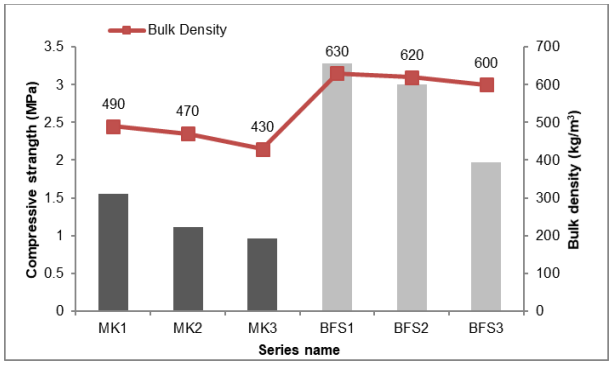

Fig. 4 - Bulk density and compressive strength results.

The high Blaine fineness value of metakaolin increased the water requirement for the consistency of the mixture and caused the decrease of the compressive strength value. The greater reactivity of the slag in comparison with MK can also, contribute to the greater strength. The apparent porosity and compressive strength data of the test samples are given in the Figure 5**.** Due to the decrease in the amount of cement, the apparent porosity values increased and the compressive strength decreased. The correlation between apparent porosity and compressive strength is quite good (R^2=0.84).

Apparent porosity data are given in the Table 3. The apparent porosity values of the series produced with metakaolin are higher than those produced BFS. With the increase in the apparent porosity value and the decrease in the amount of cement in the mixture, the bulk density and compressive strength is decreased.

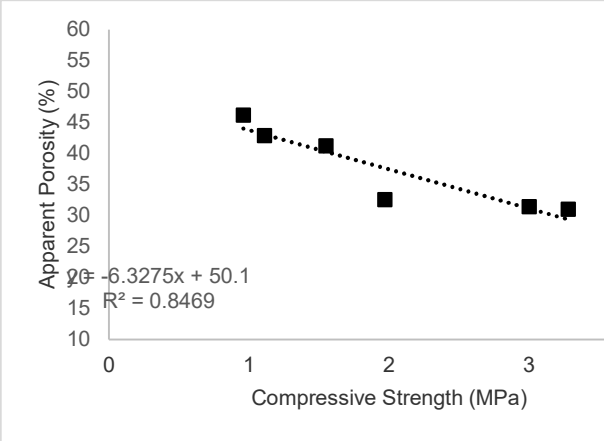

Fig. 5 - Correlation between apparent porosity and compressive strength.

Microstructure studies were carried out on the series with the highest compressive strength values. XRD analysis of the samples produced from MK1 mixture is given Figure 6. In the mineral composition of the sample, CSH, xonotlite, portlandite, mullite and quartz mineral phases were found. Tobermorite density is seen at 250 cps. SEM images show weak tobermorite plates and mullite formation that have formed in CSH gel structure (Figure 7). It can be said that the low level of tobermorite density is indicative of the fact that the silica sources present in the system are not as reactive with lime.

Table 3

Apparent porosity findings.

Series	MK1	MK2	MK3	BFS1	BFS2	BFS3
Apparent Porosity (%)	41.28	42.93	46.23	31.02	31.43	32.60

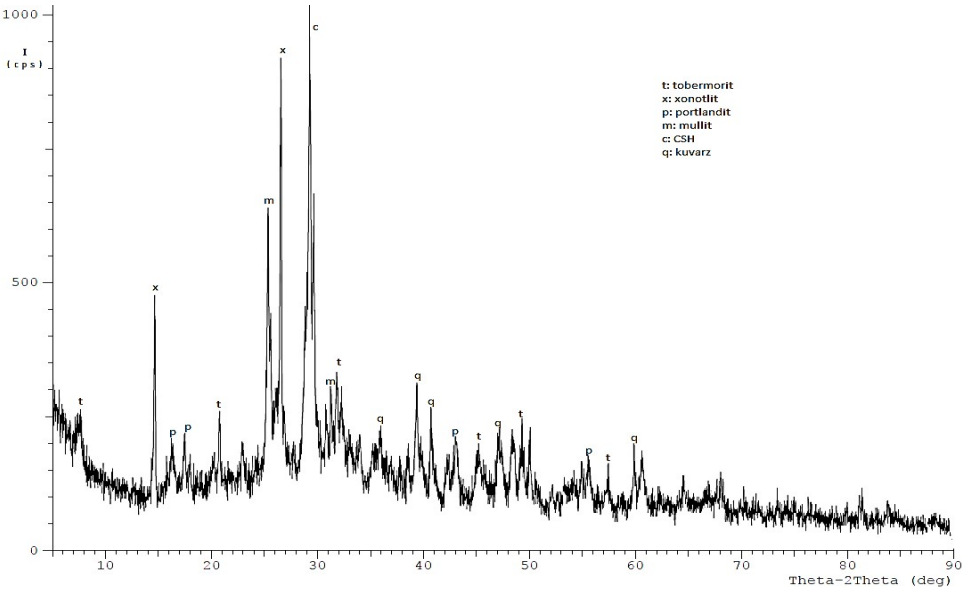

Fig. 6 - XRD analysis of MK1 samples.

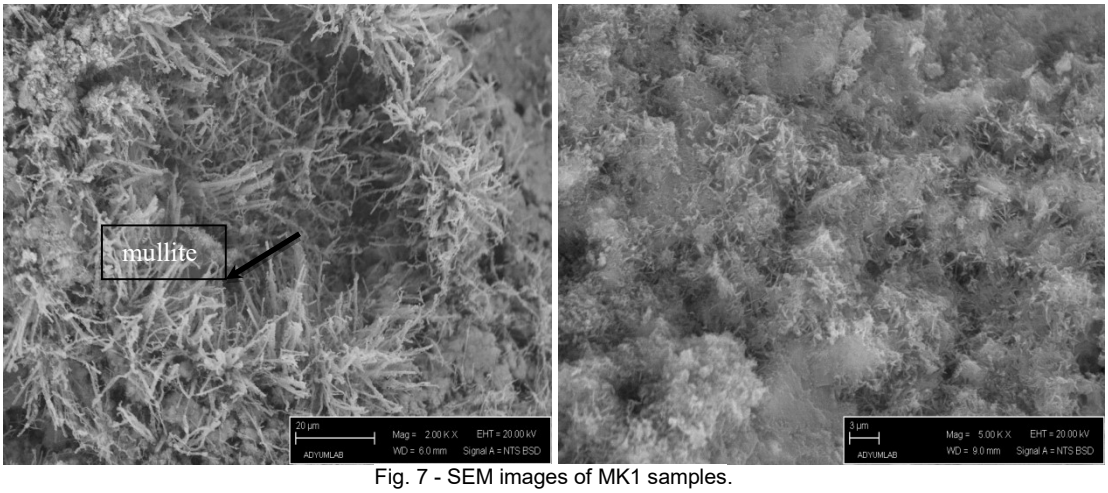

Fig. 7 - SEM images of MK1 samples.

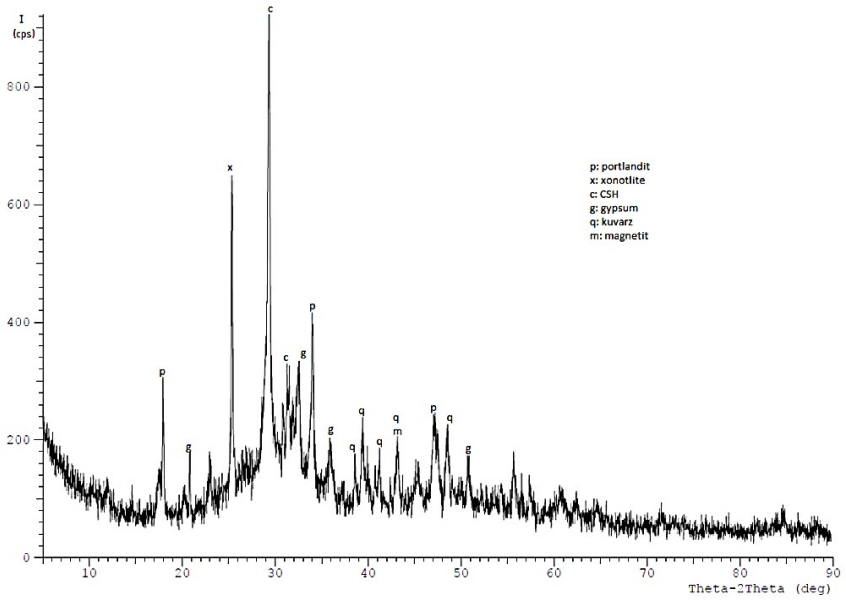

Fig. 8 - XRD analysis of BFS1 samples.

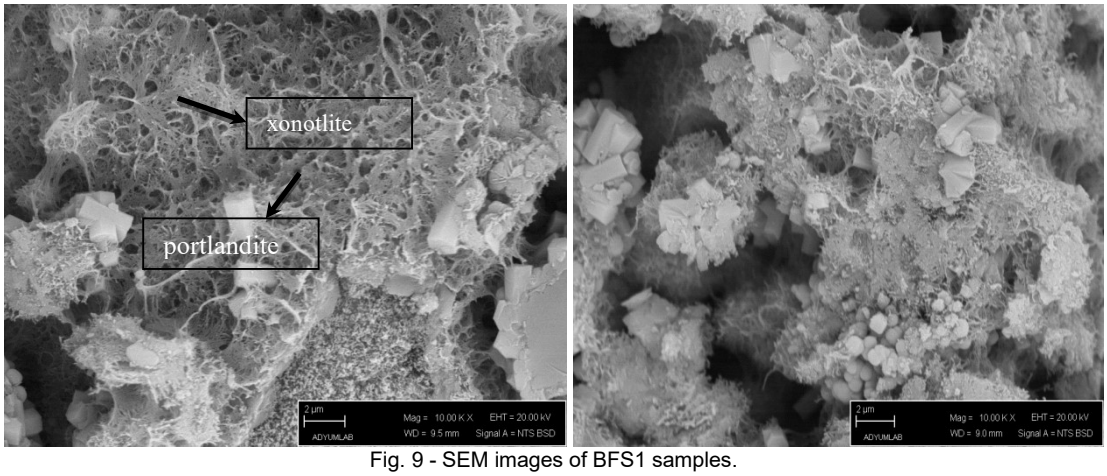

Fig. 9 - SEM images of BFS1 samples.

XRD analysis of the sample produced with blast furnace slag is given in Figure 8. In the mineralogical study, portlandite, xonotlite, CSH, gypsum, quartz and magnetite phases were found. CSH gel structure is the most important factor in the development of strength in AAC. SEM-EDX analysis of the CSH structure is given in Figure 9.

The presence of the portlandite phase in the analysis is remarkable. This phase is thought to result by the hydration of CaO in the mixture and the early hydration of the C_3S the main compound in the Portland cement.

Table 4

Thermal conductivity coefficient values

Series of samples	Place of measurement	Measurement 1	Measurement 2	Measurement 3
MK1	Front sides	0.146	0.148	0.148
	Back sides	0.126	0.126	0.123
	Average (W/mK)	**0.136**		
BFS1	Front sides	0.121	0.120	0.121
	Back sides	0.129	0.129	0.144
	Average (W/mK)	**0.127**		

The thermal conductivity coefficient studies were performed on the series with the highest compressive strengths. Measurements were made on samples with dimensions of 2x5x10 cm with a KEM QTM 500 instrument capable of measuring at a temperature range of -10 - 200 °C and a measurement range of 0,023-11,63 W/m.K. The thermal conductivity coefficients of the samples were determined by taking three measurements from the front and back sides. The measured values of the samples and their averages are given in Table 4.

The stagnant air in the pores has little thermal conductivity. Also, as the amount of pores increases, the bulk density of the material decreases. As the bulk density decreases, the thermal conductivity value also decreases. However, when the bulk density and thermal conductivity coefficients of the MK1 and BFS1 series are compared in Table 3, the situation is exactly the opposite. As the bulk density increased, the thermal conductivity coefficient decreased. This is thought to be related to the different density of metakaolin and blast furnace slag and the thickness of the shells (walls) that make up the pores in the macropores.

4. Conclusions

The results show that metakaolin and blast furnace slag can be used in the production of AAC. Silica sand used in the production of AAC is obtained from nature. For this reason, the natural environment is led to destruction and energy consumption is important. In 2018, about 2.9 million tons of BFS was produced from 3 integrated facilities operating in Turkey [24]. The recycling of BFS in the production of AAC will contribute to the protection of the natural environment as well as economic added value. Experimental studies with metakaolin have at suitable calcinations temperatures and more fine grain size grinding is expected to be useful.

Acknowledgements

Authors wish to thanks to OYAK and BAPK unit of Afyon Kocatepe University which allows the financial support under project number 15. FENBİL. 21.

REFERENCES

[1] Li Z., Chen L., Fang Q., Hao H., Zhang Y., Chen W., Xiang H., Bao, Q., Study of autoclaved aerated concrete masonry walls under vented gas explosions, Engineering Structures, 2017, **141**, 444–460.

[2] Narayanan N., Ramamurthy K., Structure and properties of aerated concrete: a review, Cement and Concrete Research, 2000, **22**, 321–329.

[3] Yuan B., Straub C., Segers S., Lu Q., L. Brouwers, H. J. H., Sodium carbonate activated slag as cement replacement in autoclaved aerated concrete, Ceramics International, 2017, **43**, 6039–6047.

[4] Kurama H., Topçu İ.B., Karakurt C., Properties of the autoclaved aerated concrete produced from coal bottom ash, Journal of Material Processing Technology, 2009, **209**, 136-144.

[5] Wongkeo W., Thongsanitgarn P., Pimraksa K., Chaipanich A., Compressive strength, flexural strength and thermal conductivity of autoclaved concrete block made using bottom ash as cement replacement materials, Materials and Design, 2012, **35**, 434-439.

[6] Rozycka A., Pichor W., Effect of perlite waste addition on the properties of autoclaved aerated concrete, Construction and Building Materials, 2016, **120**, 65–71.

[7] Owsiak Z., Soltys A., Sztaboroski P., Mazur, M., Properties of autoclaved aerated concrete with halloysite under industrial conditions, Procedia Engineering, 2015, **108**, 214 – 219.

[8] Qu X., Zhao X., Previous and present investigations on the components, microstructure and main properties of autoclaved aerated concrete – A review, Construction and Building Materials, 2017, **135**, 505–516.

[9] Hassan A., Lachemi M., Hossain K., Effect of metakaolin and silica fume on the durability of self-consolidating concrete, Cement & Concrete Composites, 2012, **34**, 801–807.

[10] Shi Z., Shui Z., Li Q., Geng H., Combined effect of metakaolin and sea water on performance and microstructures of concrete, Construction and Building Materials, 2015, **74**, 57–64.

[11] Nikhila J., Kumar C., Partial replacement of cement with metakaolin in high strength concrete", Int. J. Engg. Res. & Sci. & Tech., 2015, **4**(4), 336-349.

[12] Tokyay M., Cement and Concrete Mineral Admixtures. CRC Press, London, UK. 2016.

[13] Patra K.R., Mukharjee B.B., Influence of incorporation of granulated blast furnace slag as replacement of fine aggregate on properties of concrete, Journal of Cleaner Production, 2017, **165**, 468-476.

[14] Güçlüer K., Ünal O., Demir İ., Başpınar M.S., An investigation of steam curing pressure effect on pozzolan additive autoclaved aerated concrete, TEM Journal, 2015, **4**(1), 78-82.

[15] Kunchariyakun K., Asavapisit S., Sombatsompop K., Properties of autoclaved aerated concrete incorporating rice husk ash as partial replacement for fine aggregate, Cement & Concrete Composites, 2015, **55**,11–16.

[16] Walczak P., Małolepszy J., Reben M., Szymański P., Rzepa K., Utilization of waste glass in autoclaved aerated concrete, Procedia Engineering, 2015,**122**, 302 – 309.

[17] Huang X., Ni W., Cui W., Wang Z., Zhu L., Preparation of autoclaved aerated concrete using copper tailings and blast furnace slag, Construction and Building Materials, 2012, **27**, 1–5.

[18] Başpınar M.S., Demir İ., Kahraman E., Görhan G., Utilization potential of fly ash together with silica fume in autoclaved aerated concrete production, KSCE Journal of Civil Engineering,2014, **18**(1), 47-52.

[19] TS EN 197-1, Çimento - Bölüm 1: Genel Çimentolar - Bileşim, Özellikler ve Uygunluk Kriterleri. Türk Standartları Enstitüsü, Ankara, 2002.

[20] ASTM C1113 / C1113M-09. Standard Test Method for Thermal Conductivity of Refractories by Hot Wire (Platinum Resistance Thermometer Technique), ASTM International, West Conshohocken, PA., 2009.

[21] TS EN 772-4, Kagir Birimler, deney metotları- Bölüm 4: Tabii Taş Kâgir Birimlerin Toplam Ve Görünen Porozitesi Ile Boşluksuz Ve Boşluklu Birim Hacim Kütlesinin Tayini. Türk Standartları Enstitüsü, Ankara, 2000.

[22] Tada S., Material design of aerated concrete—An optimum performance design, Materials and Structures, 1986, **19**(1), 21-26.

[23] Song Y., Li B., Yang E.H., Liu Y., Ding T., Feasibility study on utilization of municipal solid waste incineration bottom ash as aerating agent for the production of autoclaved aerated concrete, Cement and Concrete Composites, 2015, **56**, 51-58.

[24] TÇÜD, Iron and Steel Slag Report, Steel Producers Association of Turkey, 2019.

****

****